# Supporting Information for *The Role of Mesoscale Cloud Morphology in the Shortwave Cloud Feedback*

Isabel L. McCoy[1,2], Daniel T. McCoy[3], Robert Wood[4], Paquita Zuidema[2], and Frida A. -M. Bender[5]

[1]Cooperative Programs for the Advancement of Earth System Science, University Corporation for Atmospheric Research, Boulder, CO, 80307-3000, USA

[2]Department of Atmospheric Sciences, Rosenstiel School, University of Miami, Miami, FL, 33149-1031, USA

[3]Department of Atmospheric Science, University of Wyoming, 1000 E. University Ave., Laramie, WY 82071, USA

[4]Atmospheric Sciences Department, University of Washington, Seattle, WA, 98195-1640, USA

[5]Department of Meteorology and Bolin Centre for Climate Research, Stockholm University, Stockholm Sweden

**Contents of this file**

1. Text S1 to S2
2. Table S1
3. Figures S1 to S10

**Text S1.** We can examine the predicted changes in CMIP6 models (Figure S2, S3) in more detail to determine if the responses are i) consistent across models and ii) similar to the large-scale changes estimated in previous studies. Individual CMIP6 models behave similarly to each other (Figure S3, S4) with small multi-model standard deviations (Figure S5a, d) especially when scaled by their multi-model mean (O∼0.5, Figure S5c, d). Small differences between model responses in $\Delta M/\Delta T$ can be seen in regions where the details of ocean-atmosphere interactions likely vary between models (Figure S5d). Similarly, $\Delta SST/\Delta T$ exhibits the largest model differences in the region of the North Atlantic subploar gyre (e.g., Borchert et al., 2021; Carmo-Costa et al., 2022) (Figure S5c).

We can particularly contrast the CMIP6 tendencies from this subset of GCMs with the CMIP5 $abrupt4\times CO_2$ simulation results in Qu, Hall, Klein, and Caldwell (2014b). Comparing to their Figure 9, we can look at the typical behavior of temperature mediated (scaled by the change in tropical air temperature) estimated inversion strength (EIS) and surface temperature (SST) focusing on the early stage (first 30 years) which experiences the largest response. We can estimate EIS from M and $\Delta T_{air-sea} = SST - T_{2m}$ using the $M \approx \Delta T_{air-sea} - EIS +$ constant relationship from I. L. McCoy, Wood, and Fletcher (2017). In general, the global increase in $\Delta EIS/\Delta T$ which is emphasized in sub-tropical decks (Figure S6a) and the global increase in $\Delta SST/\Delta T$ with larger increases at the high-latitudes (Figure S2a) agrees with expected behavior under climate change (e.g., Qu et al., 2014b). The regionally varying although generally decreasing $\Delta M/\Delta T$ follows from this, with the large North Atlantic decrease associated with strong weakening of marine cold air outbreaks consistent with expectations (e.g., Kolstad & Bracegirdle, 2008) (Figure S2b). We can also examine the expanded Klein-Hartmann boxes (Klein & Hartmann, 1993; Qu et al., 2014a, 2015) in more detail, which capture a range of MCC cloud morphologies in key sub-tropical regions (Figure S1, S6a). Multi-model changes are consistent in behavior with earlier studies (Qu et al., 2014b). Individual models agree in sign across regions and regional multi-model means are within 25-75% of each other (Figure Sb-e).


0094-8276/22/$5.00

In summary, these investigations into the CMIP6 predictions under $abrupt4\times CO_2$ simulations indicate that the changes in large-scale environment predicted by this set of 11 CMIP6 models are consistent with the behaviors expected by prior studies. The multi-model mean values of $\Delta M/\Delta T$ and $\Delta SST/\Delta T$ shown in Figure S2a, b are thus reasonable to use in our analysis.

**Text S2.** The multiple linear regressions used in Equations 2 and 3 of the main text are weighted by the number of observations in each bin. For reliability, only bins where there is a sufficient number of all MCC identifications ($N_{Total} \geq 500$) and closed MCC identifications ($N_{Closed} \geq 100$) are included in the fits. Because of the split-fit formulation in Equation 3, it was also necessary to apply bootstrapping for uncertainty estimation. Fits are bootstrapped with replacement (×5000) from the original $\Delta f_{Closed}$-M-SST matrix from Figure 2a. The explained variance of both regressions is high ($R^2$=0.99). Mean and standard deviation of coefficients (calculated over all 5000 bootstrapped fits) for Equations 2, 3 are provided in Table S1.

We additionally checked for collinearity between predictors (bins of M, SST where $N_{Total} \geq 500$, $N_{Closed} \geq 100$) and found that it was minimal as the correlation was very low. For all input data (Equation 2), $R^2$=0.034. For Equation 3, $R^2$=0.04 for the data subset where $SST > 290$ K and 0.03 for $SST \leq 290$ K. All of these correlations are well below the $R^2$=0.9 threshold where predictor collinearity becomes an issue (Qu et al., 2015; D. T. McCoy et al., 2022).

## References

Borchert, L. F., Menary, M. B., Swingedouw, D., Sgubin, G., Hermanson, L., & Mignot, J. (2021, February). Improved Decadal Predictions of North Atlantic Subpolar Gyre SST in CMIP6. *Geophysical Research Letters*, *48*(3). Retrieved 2022-06-30, from `https://onlinelibrary.wiley.com/doi/10.1029/2020GL091307` doi: 10.1029/2020GL091307

Carmo-Costa, T., Bilbao, R., Ortega, P., Teles-Machado, A., & Dutra, E. (2022, March). Trends, variability and predictive skill of the ocean heat content in North Atlantic: an analysis with the EC-Earth3 model. *Climate Dynamics*, *58*(5-6), 1311–1328. Retrieved 2022-06-30, from `https://link.springer.com/10.1007/s00382-021-05962-y` doi: 10.1007/s00382-021-05962-y

Klein, S. A., & Hartmann, D. L. (1993, August). The Seasonal Cycle of Low Stratiform Clouds. *Journal of Climate*, *6*(8), 1587–1606. doi: 10.1175/1520-0442(1993)006⟨1587:tscols⟩2.0.co;2

Kolstad, E. W., & Bracegirdle, T. J. (2008, June). Marine cold-air outbreaks in the future: an assessment of IPCC AR4 model results for the Northern Hemisphere. *Climate Dynamics*, *30*(7-8), 871–885. doi: 10.1007/s00382-007-0331-0

McCoy, D. T., Field, P., Frazer, M. E., Zelinka, M. D., Elsaesser, G. S., Mülmenstädt, J., ... Lebo, Z. J. (2022, April). Extratropical Shortwave Cloud Feedbacks in the Context of the Global Circulation and Hydrological Cycle. *Geophysical Research Letters*, *49*(8). Retrieved 2022-07-01, from https://onlinelibrary.wiley.com/doi/10.1029/2021GL097154 doi: 10.1029/2021GL097154

McCoy, I. L., Wood, R., & Fletcher, J. K. (2017, November). Identifying Meteorological Controls on Open and Closed Mesoscale Cellular Convection Associated with Marine Cold Air Outbreaks. *Journal of Geophysical Research-Atmospheres*, *122*(21), 11678–11702. doi: 10.1002/2017jd027031

Myers, T. A., Mechoso, C. R., Cesana, G. V., DeFlorio, M. J., & Waliser, D. E. (2018). Cloud Feedback Key to Marine Heatwave off Baja California. *Geophysical Research Letters*, *45*(9), 4345–4352. doi: 10.1029/2018gl078242

Myers, T. A., Scott, R. C., Zelinka, M. D., Klein, S. A., Norris, J. R., & Caldwell, P. M. (2021). Observational constraints on low cloud feedback reduce uncertainty of climate sensitivity. *Nature Climate Change*. doi: 10.1038/s41558-021-01039-0

Pincus, R., Hubanks, P. A., & Platnick, S. (2020). MODIS Standard L3 MCD06 COSP Product. *Science Investigator-led Processing System, Goddard Space Flight Center*. (Dataset (Accessed April 2021)) doi: 10.5067/MODIS/MCD06COSP_D3_MODIS.062

Qu, X., Hall, A., Klein, S. A., & Caldwell, P. M. (2014a, May). On the spread of changes in marine low cloud cover in climate model simulations of the 21st century. *Climate Dynamics*, *42*(9-10), 2603–2626. doi: 10.1007/s00382-013-1945-z

Qu, X., Hall, A., Klein, S. A., & Caldwell, P. M. (2014b). The strength of the tropical inversion and its response to climate change in 18 CMIP5 models. *Climate Dynamics*, *45*(1-2), 375–396. doi: 10.1007/s00382-014-2441-9

Qu, X., Hall, A., Klein, S. A., & DeAngelis, A. M. (2015, September). Positive tropical marine low-cloud cover feedback inferred from cloud-controlling factors. *Geophysical Research Letters*, *42*(18), 7767–7775. doi: 10.1002/2015gl065627

Schmeisser, L., Bond, N. A., Siedlecki, S. A., & Ackerman, T. P. (2019). The Role of Clouds and Surface Heat Fluxes in the Maintenance of the 2013–2016 Northeast Pacific Marine Heatwave. *Journal of Geophysical Research: Atmospheres*, *124*(20), 10772–10783. doi: 10.1029/2019jd030780

Scott, R. C., Myers, T. A., Norris, J. R., Zelinka, M. D., Klein, S. A., Sun, M., & Doelling, D. R. (2020). Observed Sensitivity of Low-Cloud Radiative Effects to Meteorological Perturbations over the Global Oceans. *Journal of Climate*, *33*(18), 7717–7734. doi: 10.1175/jcli-d-19-1028.1

**Table S1.** Mean and Standard Deviations of Regression Coefficients for Equations 2 and 3[a,b]

| Fit | $a$ (K$^{-1}$) | $b$ (K$^{-1}$) | $c$ |
|---|---|---|---|
| *Total* | -0.0269±0.0003 | -0.0161±0.0002 | 4.64±0.05 |
| $SST > 290$ K | -0.0230±0.0004 | -0.0145±0.0004 | 4.19±0.12 |
| $SST \leq 290$ K | -0.0322±0.0002 | -0.0165±0.0002 | 4.69±0.05 |

[a] Fits of $f_{Closed} - M - SST$ data (Figure 2a) generally take the form: $f_{Closed} = a \cdot M + b \cdot SST + c$.

[b] Equation 2 uses coefficients from row 1, Equation 3 uses coefficients from rows 2 and 3.

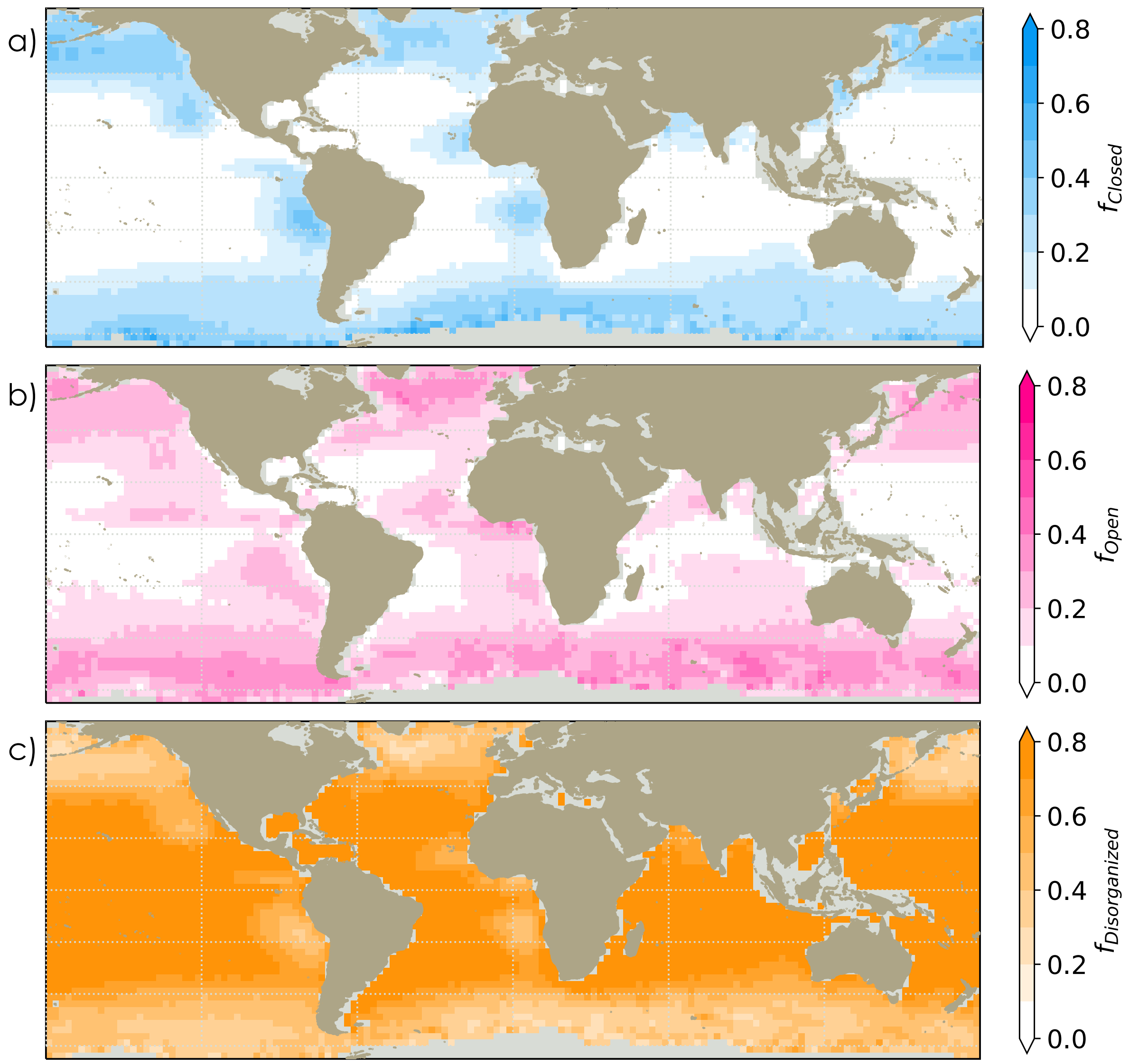


**Figure S1.** Annual mean MIDAS cloud morphology relative occurrence frequencies for 2003-2018: a) closed, b) open, and c) cellular but disorganized MCC.

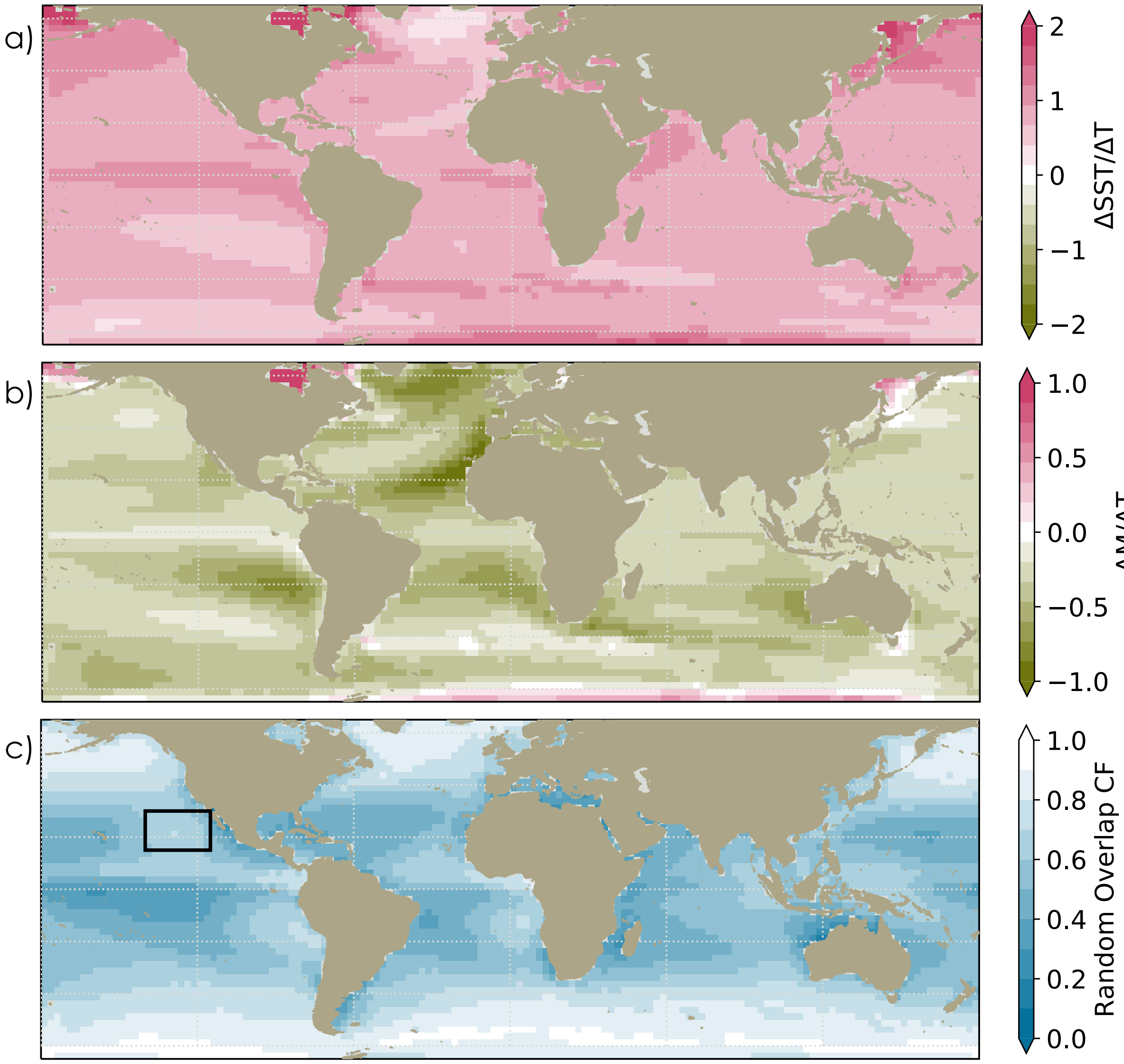


**Figure S2.** CMIP6 simulated change from *piControl* to *abrupt*$4 \times CO_2$ in a) sea surface temperature (SST) and b) lower tropospheric stability (as measured by the marine cold air outbreak index, M) per degree of global warming (measured by area-weighted change in 2 m air temperature, $\Delta T$). c) Annual mean estimate of random-overlapped low cloud fraction from the MODIS cloud mask (Pincus et al., 2020), following Scott et al. (2020). The black box in c) shows the out-of-sample test region (15-30°N, 140-115°W) where a marine heatwave was influential between November 2013-January 2016 (Myers et al., 2018; Schmeisser et al., 2019; Myers et al., 2021).

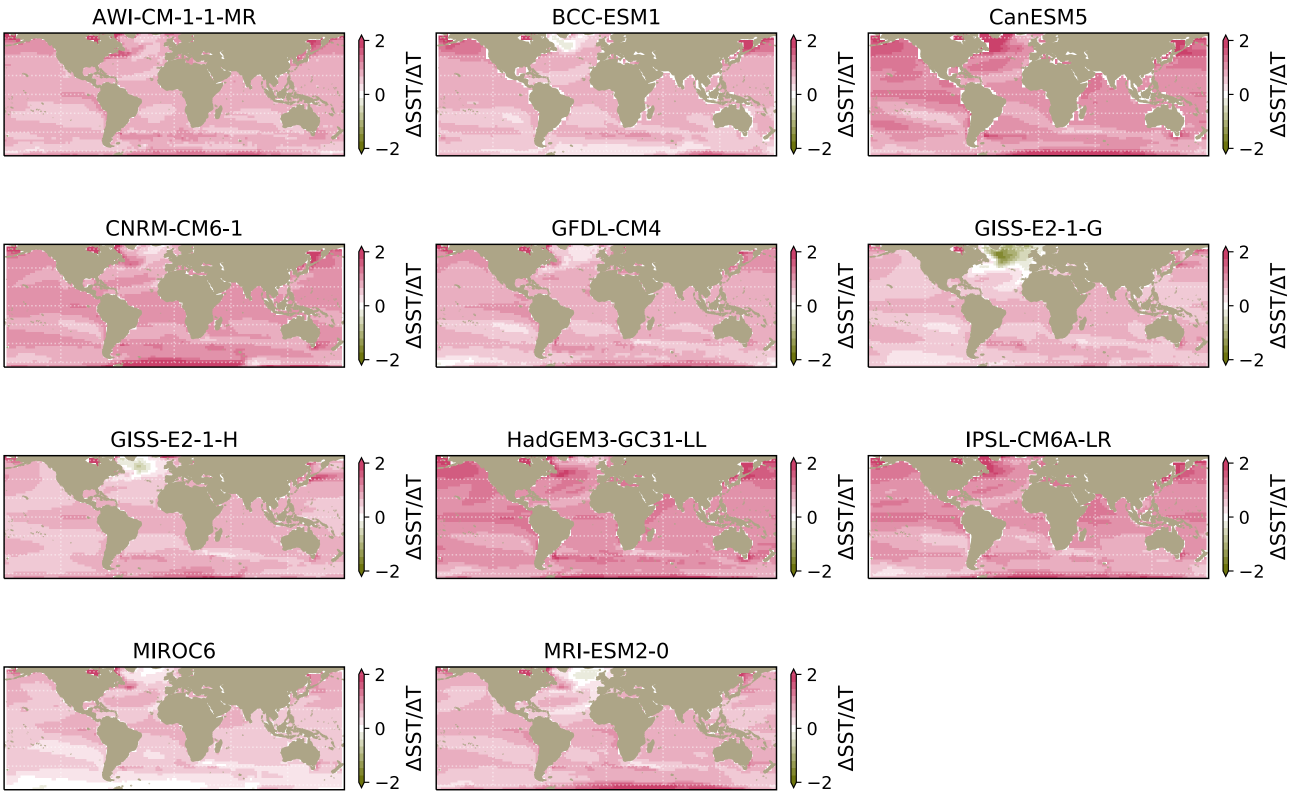


**Figure S3.** Simulated $\Delta SST/\Delta T$ for individual CMIP6 models contributing to the multi-model mean shown in Figure S2a.

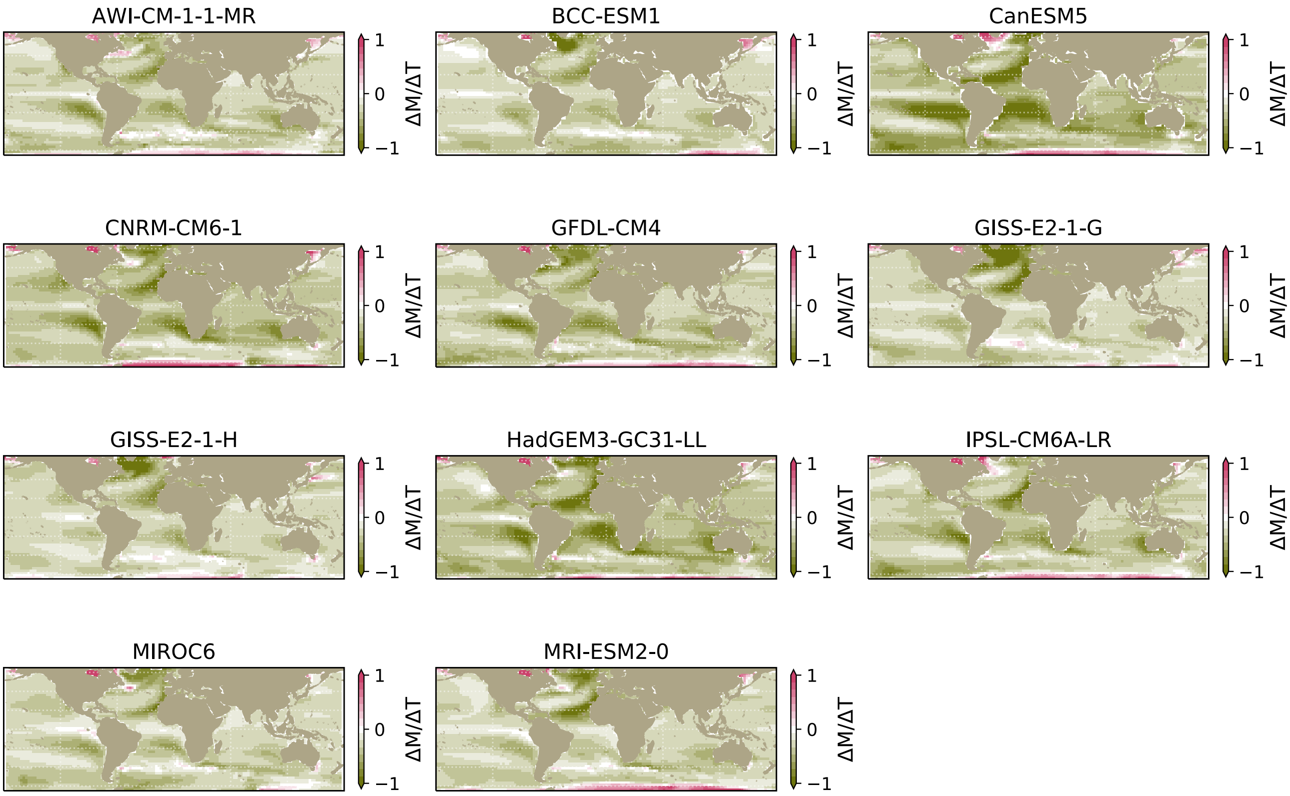


**Figure S4.** Simulated $\Delta M/\Delta T$ for individual CMIP6 models contributing to the multi-model mean shown in Figure S2b.

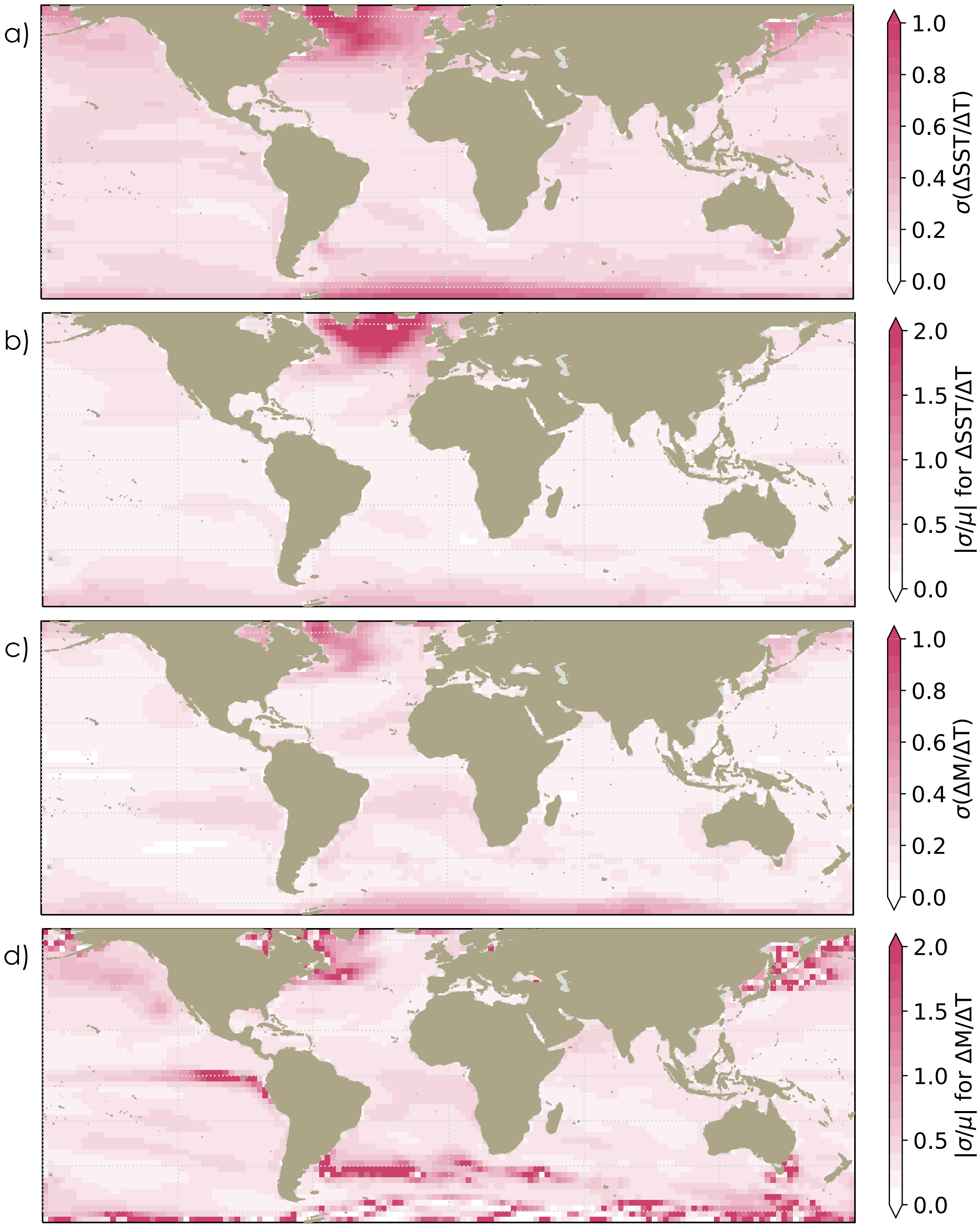


**Figure S5.** Standard deviation across individual CMIP6 model means for a) $\Delta SST/\Delta T$ and c) $\Delta M/\Delta T$. Ratio of multi model standard deviation over multi-model mean for b) $\Delta SST/\Delta T$ and d) $\Delta M/\Delta T$.

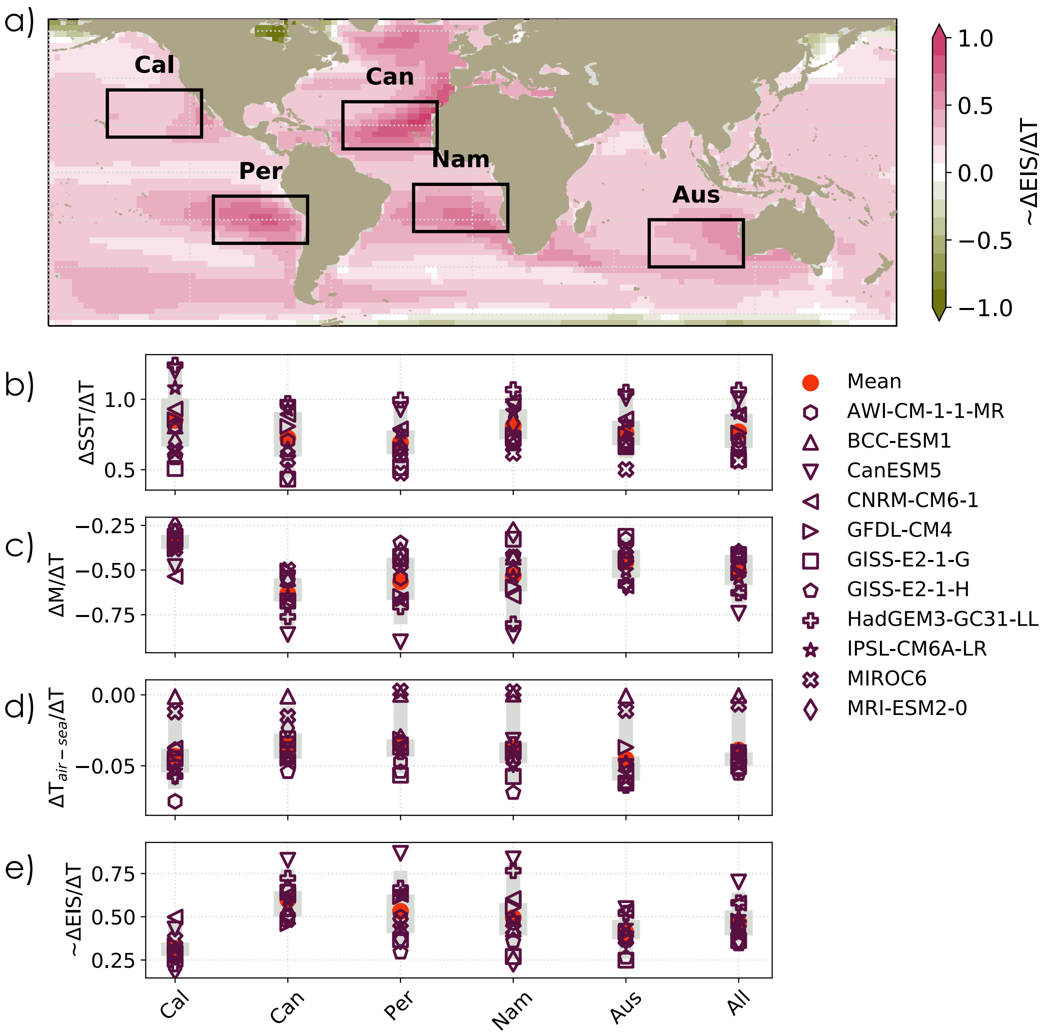


**Figure S6.** CMIP6 simulated changes for a) key subtropical regions in Qu et al. (2014a) for b) $\Delta SST/\Delta T$, c) $\Delta M/\Delta T$, d) $\Delta T_{air-sea}/\Delta T$, and e) an approximate estimate of $\Delta EIS/\Delta T$ using $M \approx \Delta T_{air-sea} - EIS +$ constant (I. L. McCoy et al., 2017). a) The multi-model mean of the approximate $\Delta EIS/\Delta T$, as in Figure S2. b-e) Individual model means (shapes) are shown with the multi-model mean (red circle), 5-95% (thin gray lines), and 25-75% (thick grey lines) for separate regional boxes in a) and the combined regional box behavior.

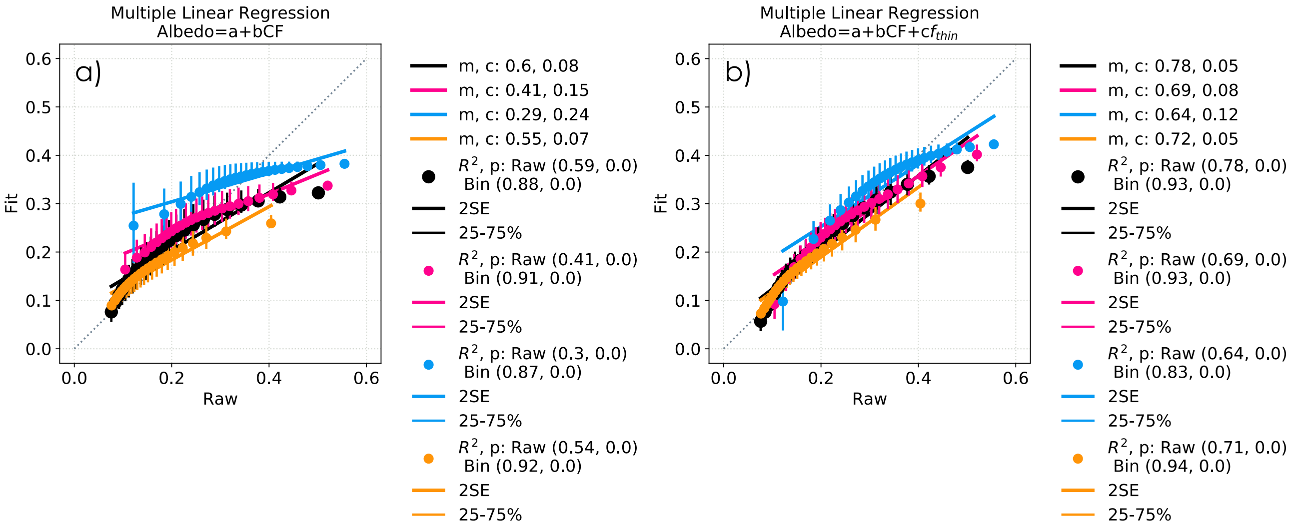


**Figure S7.** Predicting MIDAS identified scene albedo from Figure 1 using multiple linear regressions with a) CF and b) CF and $f_{thin}$ as predictors. Fit predicted albedo is shown on the y-axis and the raw scene albedo is on the x-axis. Combined total (black), closed MCC (blue), open MCC (pink), and cellular but disorganized (orange) identifications are fit separately. $R^2$ and $p$ values are shown for the individual (*Raw*) points and for the mean fitted albedo within 25 x-axis quantile bins (*Bin*). Thick lines show 2SE and thin the 25-75% range within each quantile. Slope ($m$) and intercept ($c$) are shown for the linear fit applied to the quantile bins (line). A dashed 1:1 line is included for reference. Generally, the closer $m$ is to one and $c$ is to zero, the better the prediction with the regression model, suggesting b) captures more of albedo behavior than a).

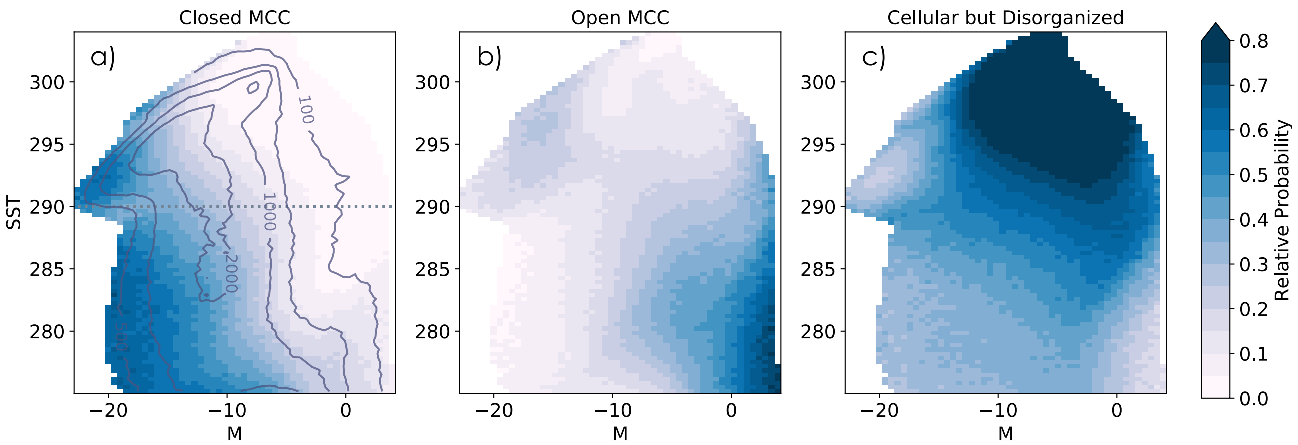


**Figure S8.** As in Figure 2a-c but for the full MIDAS period (2003-2018): the MIDAS relative occurrence frequency in the M-SST environmental phase space a) closed, b) open, and c) disorganized MCC.

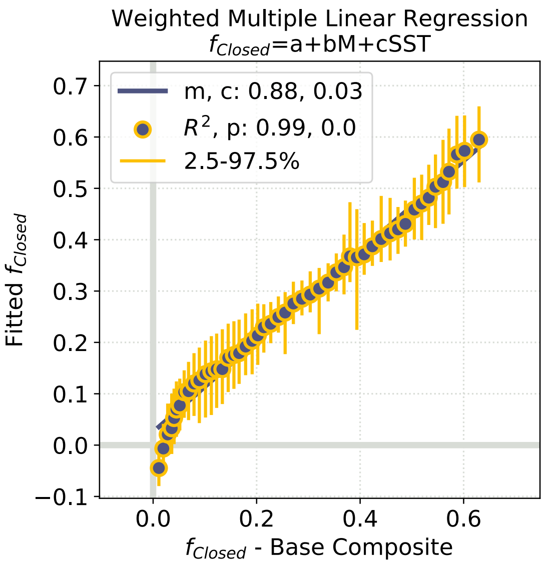


**Figure S9.** As in Figure 2d but using Equation 2 to predict $f_{Closed}$ from Figure 1a.

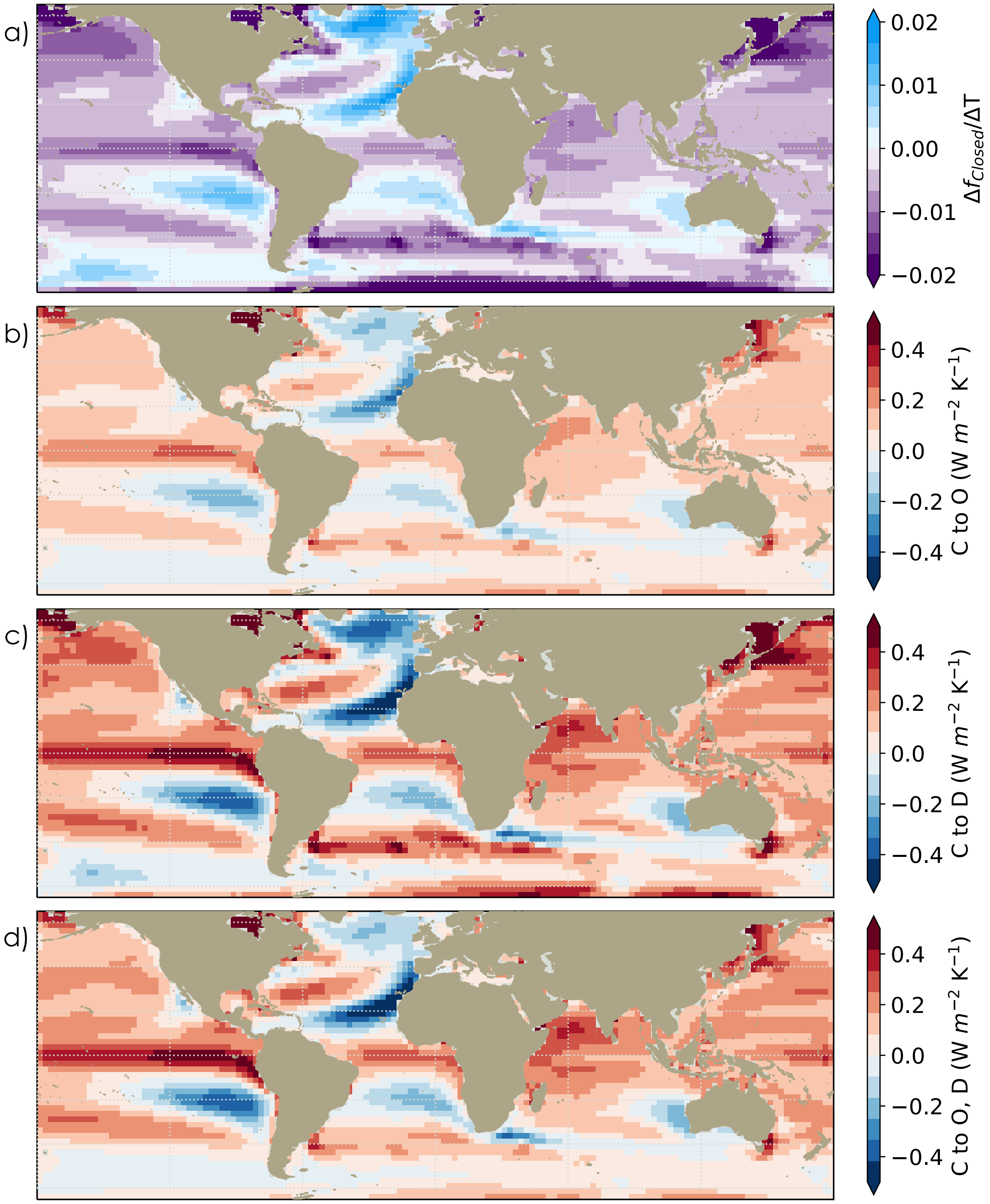


**Figure S10.** As in Figure 3 but predicted from Equation 4 using coefficients from the no-split model in Equation 2 instead of the split model in Equation 3. a) $\Delta f_{Closed}/\Delta T$ with the optical depth component of the morphology feedback per $\Delta T$ assuming closed MCC shift to b) open MCC, c) cellular but disorganized MCC, or d) an aggregate of open and disorganized MCC dependent on initial SST.